HHS Public Access

Author manuscript

IEEE Biomed Circuits Syst Conf. Author manuscript; available in PMC 2020 January 27.

Published in final edited form as:

IEEE Biomed Circuits Syst Conf. 2019 October ; 2019: . doi:10.1109/BIOCAS.2019.8919144.

Multi-Access Networking with Wireless Ultrasound-Powered Implants

Ting Chia Chang, **Max Wang**, **Amin Arbabian**

Electrical Engineering, Stanford University, Stanford, CA, 94305, USA

Abstract

Multi-access networking with miniaturized wireless implantable devices can enable and advance closed-loop medical applications to deliver precise diagnosis and treatment. Using ultrasound (US) for wireless implant systems is an advantageous approach as US can beamform with high spatial resolution to efficiently power and address multiple implants in the network. To demonstrate these capabilities, we use wirelessly powered mm-sized implants with bidirectional communication links; uplink data communication measurements are performed using time, spatial, and frequency-division multiplexing schemes in tissue phantom. A 32-channel linear transmitter array and an external receiver are used as a base station to network with two implants that are placed 6.5 cm deep and spaced less than 1 cm apart. Successful wireless powering and uplink data communication around 100 kbps with a measured bit error rate below 10^{-4} are demonstrated for all three networking schemes, validating the multi-access networking feasibility of US wireless implant systems.

Index Terms—

ultrasonic power transfer; wireless implants; beamforming; time-division multiplexing; spatial multiplexing; frequency-division multiplexing; multi-access networking

I. Introduction

Miniaturized implantable devices employing wireless power and data links are igniting new developments in chronic monitoring as well as personalized treatment [1]. DARPA has initiated the Electric Prescription program to develop minimally invasive approaches for sensing and controlling the nervous system to improve long-term health. In order to incorporate both monitoring and modulation functionality into wireless implant systems, they need to support a coordinated network between many wireless implants and a base station or a mesh network between the implants themselves. Taking overreactive bladder control as an example, a pressure monitor is needed to track bladder contraction so that stimulation can be performed on the peripheral nerves accordingly [2]. In brain machine interface applications, dense neural recording and stimulation from multiple locations are desired for precise control [3]. These tasks usually require many implant nodes working

tcchang3@stanford.edu.

together at different times or simultaneously; as a result, coordination of power transfer and data communication in wireless implant systems is essential.

Previously, we have demonstrated mm-sized US-powered implants that perform pressure monitoring [4], neural stimulation [5], or data communication [6] deep in tissue. The concept of networking using US for implants has also been discussed in [7]–[9]. In [7], code-division multi-access based on Walsh Hadamard codes was utilized for communication with three US transmitters and one US receiver. In [8], spatial degrees of freedom were explored for acoustic multiple-input multiple-output communication using quadrature phase-shift keying. However, both [7] and [8] used signal generators to drive the implanted transmitters, sidestepping the wireless powering component. In [9], wireless powering of miniaturized implants with backscattering data was shown in a time division manner, but the data rate is limited to 10s of bps in order to be compatible with traditional US imaging systems which have low frame rates.

The US wireless implant system typically consists of US-powered implants and an external US array as a base station that is able to transmit power and communicate with the implanted devices. Since the external US array is not as power-constrained as the implants, one can build in more intelligence into the array for more sophisticated data processing and control. In this paper, we use the proof-of-concept implants reported in [6] along with a base station, consisting of a customized US transmitting array and a receiver, to demonstrate three multi-access networking schemes: time, spatial, and frequency division multiplexing. For time-division multiplexing, the implants in the network power up and send uplink data at different time slots based on the control signals from the base station. In spatial multiplexing, multiple implants power up and transmit data simultaneously, increasing the data throughput. The uplink data from different implants is separated in the spatial domain. Lastly, the frequency-division multiplexing scheme uses different uplink carriers for communication. It is advantageous when the receiver at the base station cannot distinguish data spatially; it can also relax the spatial resolution design requirement for the receiver at the base station.

II. Experimental Setup

The prototype US wireless implant system is shown in Fig. 1. The previously developed 32-channel linear transmitter (TX) array is used for powering and data transmission; the array is fully programable with a Xilinx Zynq SoC to set the desired beam pattern and customize the downlink data stream [10]. A separate single element wideband external receiver (RX) with a diameter of 2.1 cm manufactured by Sonic Concepts is utilized to receive uplink data from the implants. Receive beamforming is imitated by moving the external RX via a linear stage in the x direction. The receive elements can be integrated with the TX array in the future for a more compact design as is common in US imaging or high-intensity focused ultrasound system [11].

The implant used in the experiment harvests incoming US power and simultaneously transmits on-chip pseudorandom binary sequence (PRBS) data out also using US with on-off keying modulation [6]. The implant is composed of a miniaturized TX, RX, and a chip. The

carrier frequency of uplink data is generated on-chip and is set to be about 2.6× of the input powering frequency; thus, the uplink carrier can be tuned based on the input frequency. In addition, the input fundamental and the associated harmonics are avoided such that the data can be easily processed. The data transmission starts after the implant is charged up and a notch is detected from the input envelope. The data rate is set to one tenth of the recovered clock in this proof-of-concept implant. As an example, using 0.97 MHz for wireless powering, the uplink data from the implant has a data rate of 97 kbps with a carrier frequency of 2.52 MHz. Networking with two implants is demonstrated in this paper. All transducers are immersed in a tank filled with castor oil which models the acoustic environment of tissue; the implanted RXs and TXs are all 6.5 cm away in the z direction from the external TX array and the external RX. The implanted RXs are made from PMN-PT and have dimensions of 0.9 × 0.9 × 0.5 mm with resonance close to 1 MHz. They are placed 0.9 cm apart; this distance is chosen such that the TX array can generate a beam to power up the desired implant for the target depths (lateral beamwidth is proportional to wavelength, depth and inversely proportional to aperture). The implanted TXs are built from PZT4; they are diced to 0.55 × 0.55 × 0.5 mm and have a resonance near 2.5 MHz. The same spacing of 0.9 cm is used for time and spatial multiplexing demonstrations and a closer distance of 0.3 cm is used for frequency division multiplexing in order to demonstrate simultaneous uplink even if the receiver cannot spatially differentiate the data. For measurement purposes, the chips are connected outside of the tank in order to access the terminals. RX1, TX1, and Chip1 make up Implant1; and RX2, TX2, and Chip2 make up Implant2. We will show networking with two fully-packaged miniaturized implants towards the end of the paper.

III. Wireless Measurement Results

Before networking with the implants, it is important to determine the correct focus for the array to power up the respective implants since the relative location of the TX array and the implants is unknown initially. In this section, we first show the measured results of beamforming, then we demonstrate time, spatial, and frequency division multiplexing.

A. Finding the Focus

The focus of the TX array to maximize the received power of the implanted RXs is determined by steering the US beam using all 32 elements in the xz plane while the voltages across implant RXs are monitored. With the setup in Fig. 1, setting the delay to make the array to focus at $x = -0.1$ cm and $z = 7.0$ cm (Focus1) maximizes the received power across RX1; and $x = -1.0$ cm, $z = 7.0$ cm (Focus2) makes RX2 receive the largest power (the origin is at the center of the array). The measured voltages of both RXs for the two foci as well as the unfocused case (i.e. no phase difference applied between TX elements) with 12 V applied across all TX array elements at the input frequency (f_{in}) of 0.97 MHz are shown in Fig. 2. The estimated acoustic intensity is about 0.5 mW/mm^2 for both foci. The focused power beam has a simulated half-power beamwidth of 0.34 cm. The results indicate that the focusing ability of US is able to increase the received power of the corresponding RXs by at least 4×. The measured received voltage ratios between the two RXs is higher for Focus2; this may be due to the performance mismatch between the array elements and the

characteristics of implanted RXs. In addition, a z of 7.0 cm is used for both focus settings instead of the actual distance of 6.5 cm depicted in the setup because US wave experience diffraction and attenuation in the medium which shifts the maximum intensity point to a shorter distance [12]. A more advanced methods with automatic feedback to localize implants such as real-time imaging or power level detection on the implants can be implemented in the future.

B. Time-division Multiplexing

With the correct focus determined for each implant, we perform experiments to first demonstrate networking using time-division multiplexing. This scheme is useful when the application requires information from one of the implants in the network to control and give commands to other implants. In order to demonstrate this concept, Implant1 is first powered up by setting the TX array focus to Focus1; it starts transmitting PRBS data after it is charged up and receives a notch signal from the incoming waveform. The external RX is positioned directly on top of RX1 to receive the uplink data. As seen in Fig. 3 (a), which shows the measured output voltages of the on-chip low-dropout (LDO) regulator on each implant, LDO1 rises up to about 1 V after being charged for 80 μs; LDO2, on the other hand, stays near 0 V as Implant2 does not receive sufficient US power.

We then adjust the beam from the TX array to Focus2 to power up Implant2; the external RX is also moved by 0.9 cm in the x direction to be on top of RX2 to maximize the received signal transmitted by Implant2. As expected, only LDO2 goes up to about 1 V as shown in Fig. 3 (b). The measured result demonstrates that beamforming can address implants in the network individually at different time frames without activating other ones.

Fig. 3 (c) shows the measured spectrum of received signals from the external RX for data transmitted from Implant1 (Implant2 also produces the same spectrum when Focus2 is used). The uplink carrier frequency (f_{up}) for f_{in} of 0.97 MHz is 2.52 MHz. The data rate is 97 kb/s. The modulation spectrum is not exactly symmetric around f_{up} because of the impedance profile of the implanted TXs. The received signal is passed through a finite impulse response band-pass filter and demodulated with a square-law demodulator. The eye diagram after demodulation is shown in Fig. 3 (d). The channel is mainly limited by the interference from echo and multipath. Assuming a Gaussian distribution, the signal-to-noise-and-interference ratio (SNIR) is estimated to be 17 dB from the plot; and no error is found with 10^4 bits transmitted.

C. Spatial Multiplexing

Taking advantage of the high spatial resolution provided by US, we demonstrate spatial multiplexing by powering up two implants and receiving uplink data simultaneously. The spatial multiplexing scheme can be used to communicate and obtain information from multiple implants simultaneously. In this demonstration, we split the TX array in half to generate two powering beams to power up the implants in the tank concurrently; the first 16 elements are programmed for Focus1 with an arbitrary delay of 182 μs; the rest of the TX elements are set for Focus2. An arbitrary delay is introduced to ensure the transmitted PRBS data from Implant1 and Implant2 is not correlated; the timing diagram for powering is

shown Fig. 4 (a). Additionally, since only 16 elements are used to power up each implant as opposed to all 32 elements in the time-division multiplexing demonstration, we increase the acoustic power from the array by adjusting the voltage across the TX elements to 20 V. As seen in Fig. 4 (b), measured LDO1 voltage ramps up later than LDO2 as expected because of the delay.

To distinguish receive data spatially, the external RX is moved on top of the respective implanted TXs which are 0.9 cm apart to imitate receiving beamforming. Using the same demodulation process mentioned previously, the received voltages waveforms after filtering and demodulation from both implants can be obtained, which are shown in Fig. 4 (c). Successful detection is achieved for two different data streams. Once again, no error is found with the transmission of 10^4 bits for both implants.

D. Frequency-Division Multiplexing

Although spatial multiplexing can be used to simultaneously listen to the data from multiple implants, it falls short when the external RX cannot spatially distinguish the uplink data streams because the implants are closer than the RX beamwidth. Frequency-division multiplexing can be one solution to network many implants in the aforementioned scenarios. In addition, the external RX for frequency-division multiplexing does not need to have a high spatial resolution requirement. To demonstrate the scheme in our setup, the implanted TXs are spaced closer to 0.3 cm in the tank. We again split the array in half to generate two beams to power up the implants; however, in this case, each power beam is programmed to have different f_{in} to produce different f_{up}.

Fig. 5 (a) shows the measured spectrum when f_{in} of 0.97 MHz and 1.01 MHz are used, the corresponding f_{up} are 2.52 MHz and 2.64 MHz respectively. Since f_{up} is based on f_{in} for the prototype implants, f_{up} can be easily selected by picking another f_{in} to allow more implants in the network to be accessed simultaneously. Fig. 5 (b) shows the measured spectrum when another pair of f_{in}, 0.97 MHz and 1.05 MHz, are used to power up the implants. f_{up} of 2.78 MHz is observed in the spectrum along with f_{up} of 2.52 MHz. After filtering the signal in Fig. 5 (a) at the respective f_{up} and then applying demodulation, we obtain the eye diagrams shown in Fig. 5 (c) and (d) for two data streams from Implant1 and Implant2. The difference in receive amplitude is mainly because the implanted TX used in the experiment is designed to have resonance around 2.5 MHz as mentioned in section II. It is possible to increase the signal strength by utilizing a more wideband TX on the implant or deploying a specifically designed TX for the corresponding uplink carrier.

Finally, we demonstrate frequency-division multiplexing with two *fully-packaged miniaturized implants* with a volume of 30.5 mm^3 as shown in Fig. 6 (a). The RXs on those implants are spaced 1.0 cm, while the TXs are spaced 0.4 cm. The spectrum of modulated data for f_{up} of 2.52 MHz and 2.64 MHz are clearly seen in the measured spectrum in Fig. 6 (b). In addition, the echo from the two fundamental f_{in} and the harmonics are much stronger compared to Fig. 5 (a) or (b) since the external RX is moved closer to the TX array to receive uplink data.

IV. Conclusion

We have demonstrated time, spatial, and frequency division multiplexing in tissue phantom with the US wireless implant system composed of a linear TX array, an external RX, and two prototype implants with duplex US data and power links. The uplink data for the presented multi-access schemes are successfully detected after demodulation. To further improve the performance, the data transmission protocol can be adjusted by adding identification codes to each implant, increasing the data rate, or using a 2D TX/RX array to better accommodate for a chosen multi-access scheme in the future.

Acknowledgment

This material is based upon work supported in part by the 2015 Dr. Robert Noyce Stanford Graduate Fellowship, the National Science Foundation (NSF) CAREER Award under Grant ECCS-1454107, and the NIH NIBIB under award number R01EB025867.

References

[1]. Kim J, Ghaffari R, and Kim D-H, “The quest for miniaturized soft bioelectronic devices,” Nat. Biomed. Eng, vol. 1, no. 3, pp. 1–4, 2017.

[2]. Lee JW, Kim D, Yoo S, Lee H, Lee G-H, and Nam Y, “Emerging neural stimulation technologies for bladder dysfunctions,” Int. Neurourol. J, vol. 19, no. 1, pp. 3–11, 2015. [PubMed: 25833475]

[3]. Leung VW et al., “A CMOS distributed sensor system for high-density wireless neural implants for brain-machine interfaces”, Proc. IEEE ESSCIRC, pp. 230–233, 2018.

[4]. Weber MJ, Yoshihara Y, Sawaby A, Charthad J, Chang TC, and Arbabian A, “A miniaturized single-transducer implantable pressure sensor with time-multiplexed ultrasonic data and power links,” IEEE J. Solid-State Circuits, vol. 53, no. 4, pp. 1089–1101, 4 2018.

[5]. Charthad J, Chang TC, Liu Z, Sawaby A, Weber MJ, Baker S, Gore F, Felt SA, and Arbabian A, “A mm-sized wireless implantable device for electrical stimulation of peripheral nerves,” IEEE Trans. Biomed. Circuits Syst, vol. 12, no. 2, pp. 257–270, 2018. [PubMed: 29578414]

[6]. Chang TC et al., “27.7 A 30.5mm^3 fully packaged implantable device with duplex ultrasonic data and power links achieving 95kb/s with $<10^{-4}$ BER at 8.5cm depth,” Proc. IEEE ISSCC, pp. 460–461, 2017.

[7]. Kondapalli SH, Alazzawi Y, Malinowski M, Timek T, and Chakrabartty S, “Multi-access In-vivo Biotelemetry using Sonomicrometry and M-Scan Ultrasound Imaging,” IEEE Trans. Biomed. Eng, vol. 9294, pp. 1–1, 2017.

[8]. Wang ML and Arbabian A, “Exploiting spatial degrees of freedom for high data rate ultrasound communication with implantable devices,” Appl. Phys. Lett, vol. 111, no. 133503, 2017.

[9]. Zhang Y and Shepard KL, “A 0.6-mm^2 powering and data telemetry system compatible with ultrasound b-mode imaging for freely moving biomedical sensor systems,” Proc. IEEE CICC, pp. 1–4, 2019.

[10]. Wang ML et al., “Closed-loop ultrasonic power and communication with multiple miniaturized active implantable medical devices,” Proc. IEEE IUS, pp. 1–4, 2017.

[11]. Jang JH et al., “Dual-mode integrated circuit for imaging and HIFU with 2-D CMUT arrays,” Proc. IEEE IUS, Taipei, pp. 1–4, 2015.

[12]. Goldstein A, “Steady State Spherically Focused, Circular Aperture Beam Patterns,” Ultrasound Med. Biol, vol. 32, no. 10, pp. 1441–1458, 2006. [PubMed: 17045863]

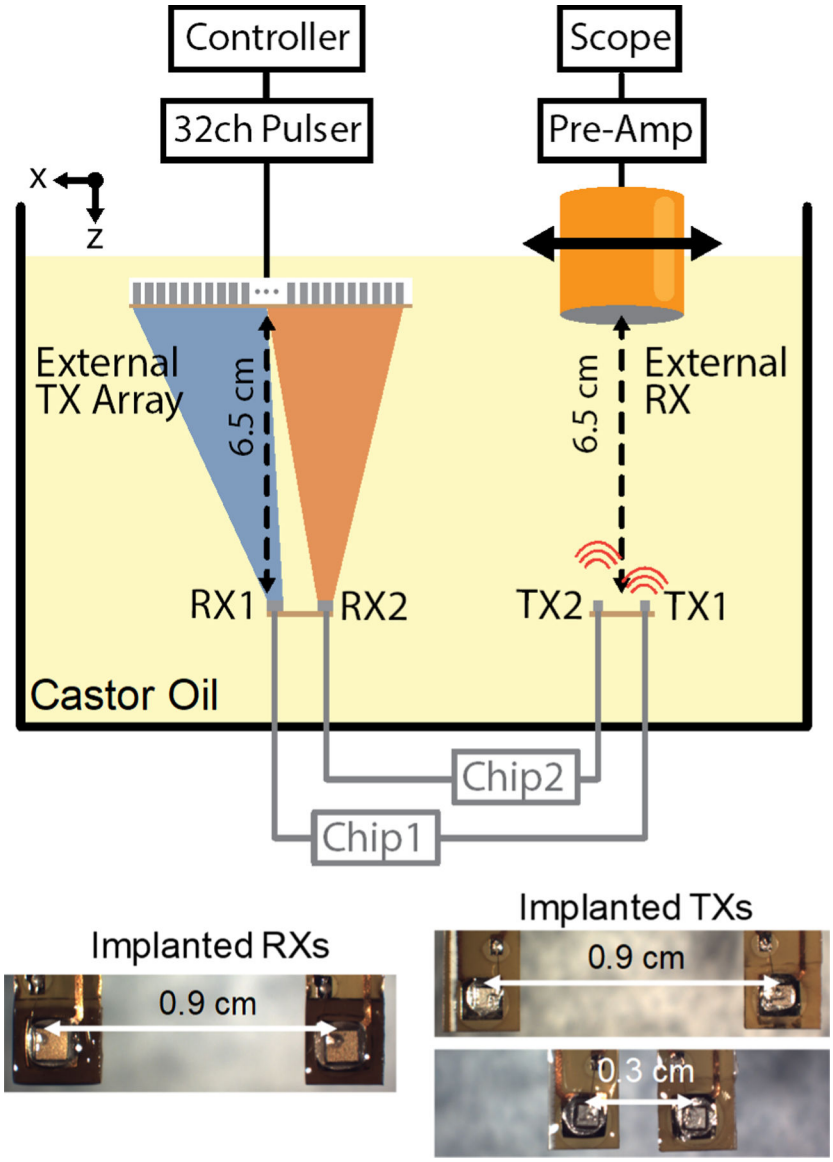

Fig. 1.

The experimental setup. The 32-channel US TX linear array and pulse are controlled by a Xilinx Zynq to adjust the US beam(s) to power up the implants. The external RX is on top of two implant TXs and is attached to a linear stage. The chips of the implants are connected externally to the corresponding transducers. Spacings between the implant transducers are shown in the photos at the bottom of the figure. Castor oil in the tank models the acoustic environment of tissue.

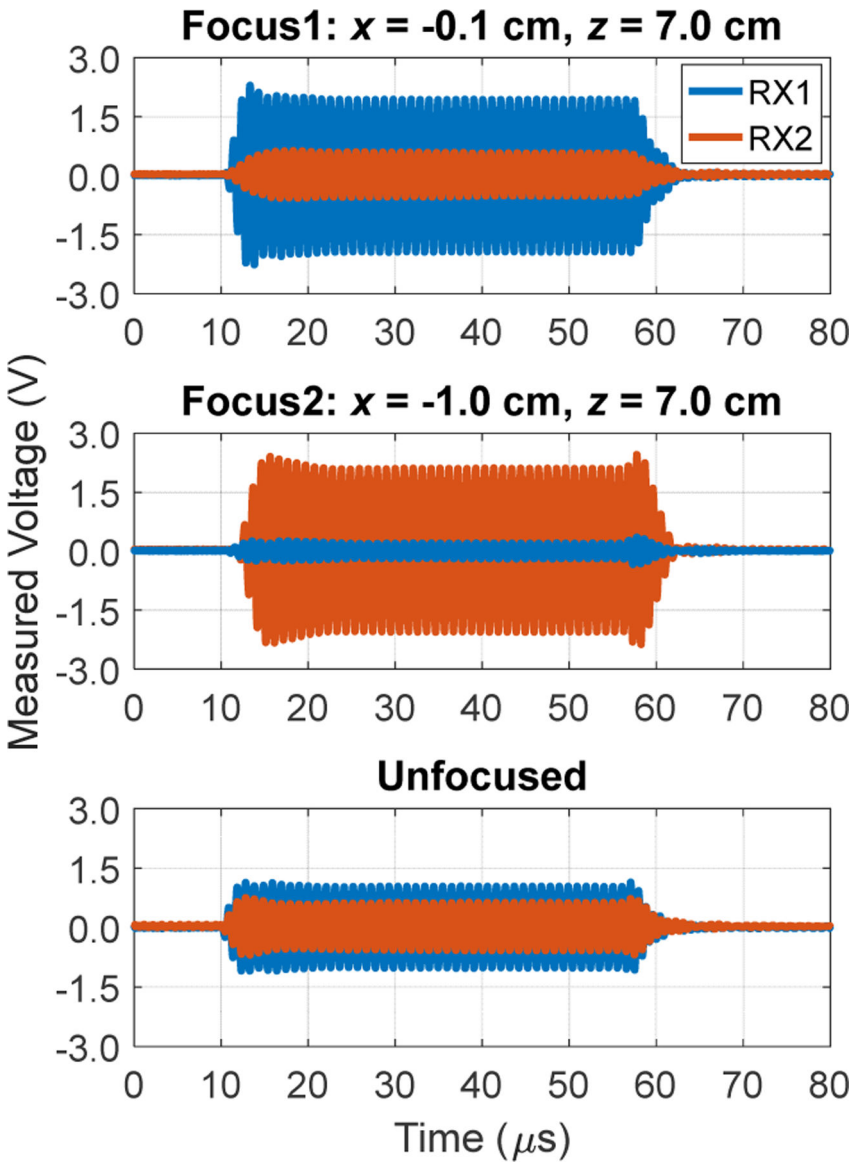

Fig. 2.

Measured received AC voltages across the implanted RX terminals for a focus on RX1 at x = −0.1cm, z = 7.0cm (Focus1, top), on RX2 at x = −1.0cm, z = 7.0cm (Focus2, middle), and when no focusing is applied (Unfocused, bottom). f_{in} is 0.97 MHz.

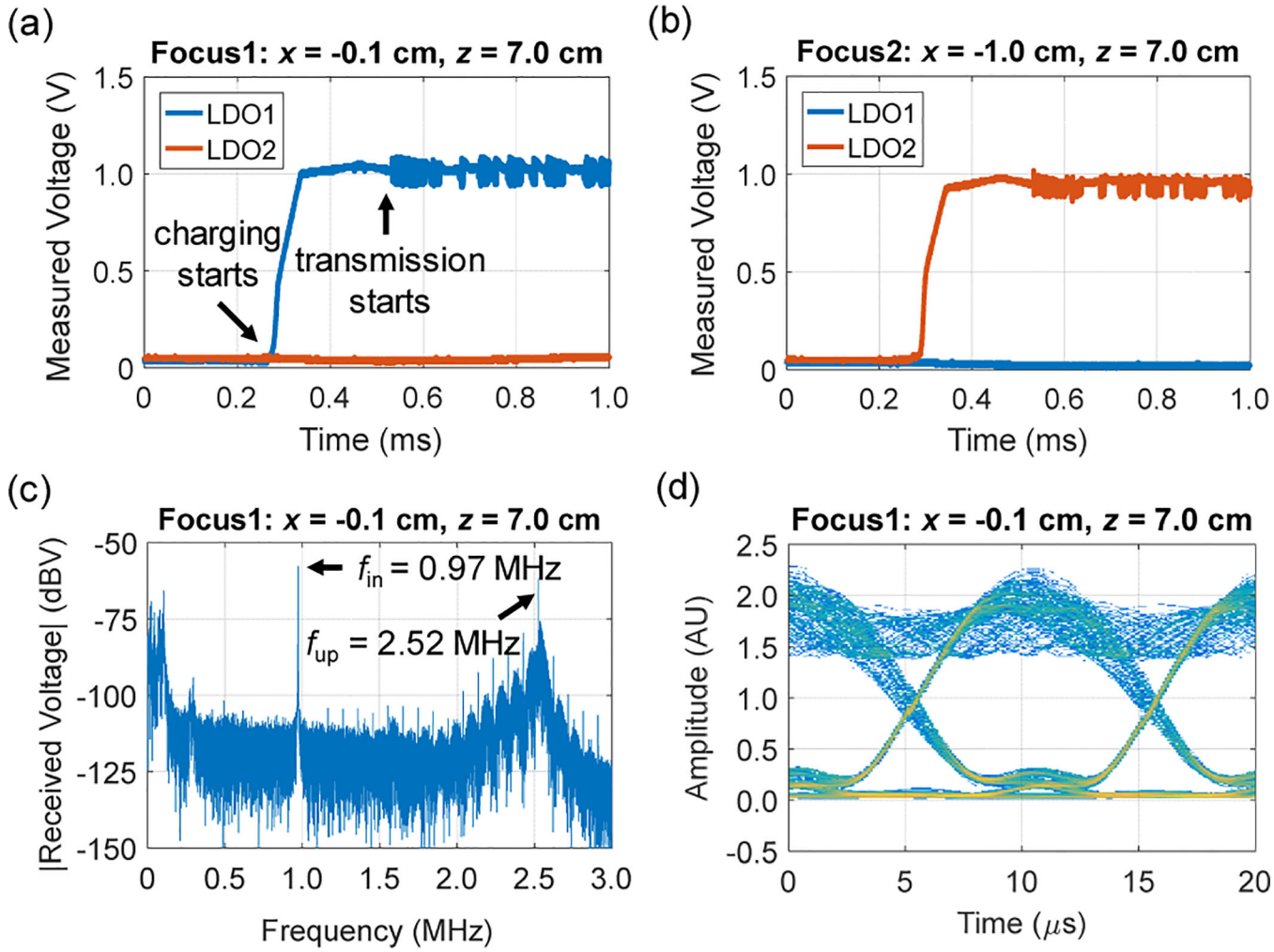

Fig. 3.

Time-division multiplexing. (a) (b) Measured LDO output voltages of the two implants when the focus of the TX array is set to Focus1 and Focus2 respectively. (c) Measured spectrum of received signals from the external RX when Focus1 is used. (d) Eye diagram of (c) after filtering and demodulation.

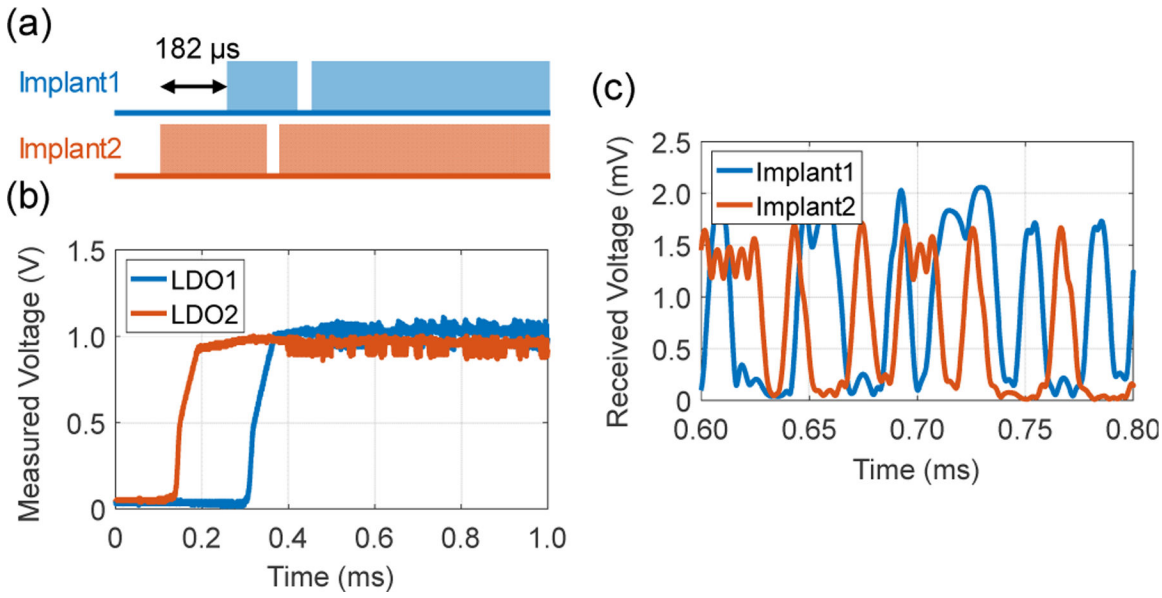

Fig. 4.

Spatial multiplexing. (a) Two implants are powered up and transmitting data simultaneously but with an arbitrary delay of 182 µs. (b) Received voltage waveforms after filtering and demodulation.

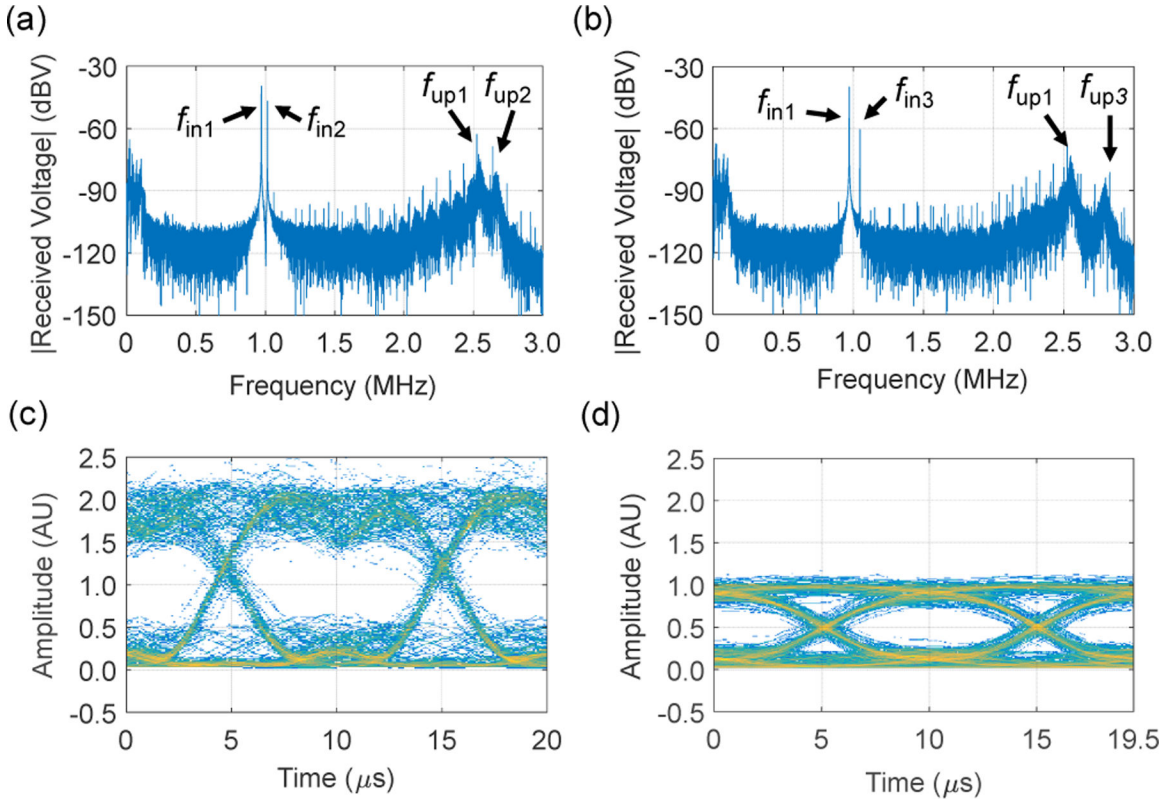

Fig. 5.

Frequency-division multiplexing. Two implants are powered up with different frequencies and two uplink data streams are received simultaneously.(a) f_{in1} = 0.97 MHz, f_{in2} = 1.01 MHz, f_{up1} = 2.52 MHz, f_{up2} = 2.64 MHz. (b) f_{in1} = 0.97 MHz, f_{in3} = 1.05 MHz, f_{up1} = 2.52 MHz, f_{up3} = 2.78 MHz. (c) (d) Eye diagrams of (a) after filtering and demodulation.

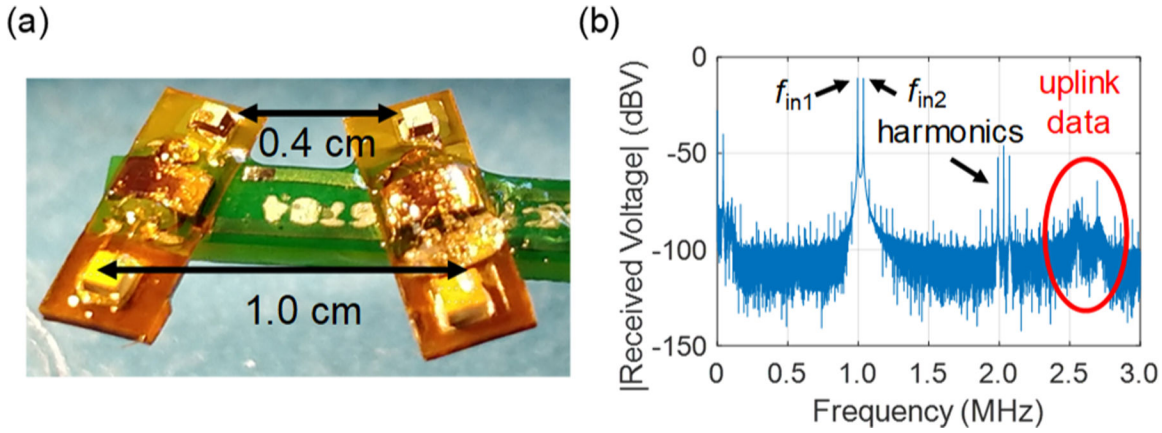

Fig. 6.

Blind frequency-division multiplexing with two fully-packaged miniaturized implants. (a) Photo of implants. (b) Measured spectrum.